Production of charm quarks in a parton cascade model for relativistic heavy ion collisions at $\sqrt{s_{NN}} = 200$ GeV

Dinesh K. Srivastava,[1,2,3,*] Steffen A. Bass,[4,†] and Rupa Chatterjee[1,‡]

[1]*Variable Energy Cyclotron Centre, HBNI, 1/AF, Bidhan Nagar, Kolkata 700064, India*

[2]*Institut für Theoretische Physik, Johann Wolfgang Goethe-Universität, Max-von-Laue-Strasse 1, D-60438 Frankfurt am Main, Germany*

[3]*ExtreMe Matter Institute (EMMI), GSI Helmholtzzentrum für Schwerionenforschung, Planckstrasse 1, 64291 Darmstadt, Germany*

[4]*Duke University, Department of Physics, 139 Science Drive, Box 90305, Durham, North Carolina 27708, USA*

(Received 23 May 2017; revised manuscript received 26 September 2017; published 27 December 2017)

We study the production and dynamics of heavy quarks in the parton cascade model for relativistic heavy ion collisions. The model is motivated by the QCD parton picture and describes the dynamics of an ultrarelativistic heavy ion collision in terms of cascading partons which undergo scattering and multiplication while propagating. We focus on the dynamics of charm quark production and evolution in $p + p$ and Au + Au collisions for several different interaction scenarios, viz., collisions only between primary partons without radiation of gluons, multiple collisions without radiation of gluons, and multiple collisions with radiation of gluons, allowing us to isolate the contributions of parton rescattering and radiation to charm production. We also discuss results of an eikonal approximation of the collision which provides a valuable comparison with minijet calculations and clearly brings out the importance of multiple collisions.

DOI: 10.1103/PhysRevC.96.064906

I. INTRODUCTION

The quark-gluon plasma (QGP), a deconfined strongly interacting matter which filled the nascent universe a few microseconds after the Big Bang, is now being routinely produced and studied in relativistic heavy ion collisions at Relativistic Heavy Ion Collider (RHIC) and the Large Hadron Collider (LHC). Its presence has been confirmed through a host of previously predicted phenomena [1–4], as well as through unexpected discoveries, such as strong elliptic flow [5,6], initial-state fluctuations leading to higher order flow [7–9] of hadrons, and phenomena related to parton recombination [10,11].

Heavy quarks serve as excellent probes of the QGP fireball as they are primarily produced by early-state hard scatterings and thus have the potential to probe the whole space-time history of the transient matter. It was generally expected that heavy quarks do not lose as much energy as light partons while traversing the quark gluon plasma due to their large mass. However, early estimates of drag and diffusion coefficients [12,13] as well as an early estimate of heavy-quark energy loss due to radiation of gluons [14] suggested that heavy quarks could possibly lose as much energy as light quarks and gluons during their passage through the QGP. These predictions have been subsequently confirmed by multiple other calculations [13,15–22], with tools ranging from simple phenomenological models used to estimate the medium modification of charm production for heavy ion collisions [23], to more detailed comparisons with models of energy loss embedded in a hydrodynamic evolution of the plasma [24]. Studies including the later hadronic stages of the evolution have also indicated that charm mesons may lose energy due to (resonant) scatterings with hadrons [25,26]. The experimental observation of large elliptic flow for D and B mesons as well as the small value of R_{AA}, the nuclear modification factor, have added experimental evidence to these findings [27,28]. Several of these aspects have been studied in great detail using the parton hadron string dynamics model at energies reached at RHIC and LHC [29–35].

In the high momentum domain, the production of heavy quarks via the interaction between (mini)jets following the initial scattering as well as due to interaction of thermal partons at high incident energies [23,36,37] has been studied. An estimate at next to leading order using the formalism developed by Mangano *et al.* [38,39] was also used to suggest [40] that angular correlations of charm-anticharm quarks in $p + p$ collisions would be drastically different for various production processes, e.g., gluon fusion or quark-antiquark annihilation, gluon splitting, and when a gluon is radiated off one of the legs of the scattering diagram. This angular correlation is expected to get even more interesting for nucleus-nucleus collisions because of the interaction of the heavy quarks with the medium.

State-of-the-art approaches for the investigation of heavy quarks in a hot and dense QCD medium need to incorporate a dynamical treatment for both the heavy quarks as well as the QCD medium. This can be either accomplished via hybrid approaches that utilize a hydrodynamic evolution for the medium in concert with a dynamical interaction model for the heavy quarks [17,24,41,42] or in the context of a purely microscopic transport for both the heavy quarks and the medium [43–45]. Parton cascade models (PCMs) [46–52] as used in this study fall into the latter category. Over the past decade, PCMs have been used for multiple studies of heavy quark dynamics in a QCD medium, ranging from the study of heavy quark energy loss in infinite matter [53] to studies of equilibration and elliptic flow built up at RHIC and LHC

*dinesh@vecc.gov.in
†bass@phy.duke.edu
‡rupa@vecc.gov.in

energies [43,45]. However, most of these studies focused on the low- to intermediate-momentum regime (mostly due to the availability of data in that regime).

As more heavy quark data at high transverse momenta become available, it is now the right time to ask whether approaches for the dynamics of heavy quarks based purely on perturbative QCD are able to describe the experimental observations in that domain. In addition, even if pQCD approaches cannot fully account for the observed features, it remains an open question to what extent the observed features of final-state observables are already imprinted on the heavy quarks prior to the formation of the QGP, i.e., via initial-state effects as well as contributions from early nonequilibrium evolution. To address these questions, we use a Monte Carlo implementation of the PCM, VNI/BMS [52], that is based on a Boltzmann transport description with pQCD matrix elements for parton-parton interactions. This particular PCM implementation also contains parton shower emission. In the present work, we discuss the implementation of heavy quarks into the PCM and calculate charm production in relativistic collisions of gold nuclei at $\sqrt{s_{NN}} = 200$ GeV. We consider several different interaction scenarios for pp and nucleus-nucleus systems, namely, an implementation of the eikonal approximation for a direct comparison with minijet calculations and to clearly demonstrate the dynamics which emerges as the partons change their momenta after collisions (which is neglected in the eikonal approximations), a scenario which involves only collisions between primary partons to clearly bring out the consequences of multiple scattering, and finally a scenario which additionally includes gluonic multiplication by radiation of gluons following scattering. The last scenario considerably increases the number of scatterings and partons (including the heavy quarks) are capable of losing energy by radiation of gluons.

II. FORMULATION

The details of the Monte Carlo implementation of the parton cascade model have been discussed in Ref. [52]. However, given how our understanding of the hot and dense QCD matter created in relativistic heavy ion collisions has changed since the inception of the PCM, a brief discussion of its past and future uses and relevancy is in order: At the time when the first parton cascade models were developed, the notion of a quark-gluon plasma was still in its infancy and it was thought of as a weakly interacting gas of quark and gluons that could be described using perturbative QCD. Having a space-time evolution based on the Boltzmann equation with quark and gluon degrees of freedom and pQCD cross sections was thought to provide a full picture of the dynamics of the deconfined system up to hadronization. With the discovery of the near perfect fluidity of the QGP at RHIC and LHC, this picture has been found to be inadequate and most PCM implementations have failed to generate the observed amount of collective flow, while utilizing pQCD-based interactions for quark and gluon degrees of freedom.[1]

However, the production of hard probes—jets, photons, and heavy quarks—can be perfectly well understood in terms of perturbative QCD production cross sections and their dynamical evolution in the early reactions stages prior to the formation of the QGP at $\tau_0 \approx 1$ fm/c is dominated by interactions with fairly large momentum transfers. Parton cascade models are thus ideally suited to describe the early out-of-equilibrium evolution of hard probes prior to the formation of a thermalized quark-gluon plasma. Their ability to describe the dynamical evolution of hard probes during the early times of the collision evolution, including multiple interactions (rescattering and gluon splitting), provides significant added insight beyond what can be gained from initial-state production Monte Carlo codes such as PYTHIA or HERWIG.[2]

Thus, we shall utilize the PCM for the study of heavy quarks during early times of Au+Au collisions at RHIC. In the following, we shall first describe the implementation of heavy quark (Q) production and interactions before moving on to our analysis.

A. Parton cascade model involving light quarks and gluons

The $2 \to 2$ scatterings included in the version of the parton cascade model utilized for our work, VNI/BMS, are

$$\begin{aligned} &q_i q_j \to q_i q_j, \quad q_i \bar{q}_i \to q_j \bar{q}_j, \\ &q_i \bar{q}_i \to gg, \quad q_i \bar{q}_i \to g\gamma, \\ &q \bar{q}_i \to \gamma\gamma, \quad q_i g \to q_i g, \\ &q_i g \to q_i \gamma, \quad gg \to q_i \bar{q}_i, \\ &gg \to gg. \end{aligned} \tag{1}$$

The $2 \to 3$ reactions are included via timelike branchings of the final-state partons:

$$\begin{aligned} &g^* \to q_i \bar{q}_i, \quad {q_i}^* \to q_i g, \\ &g^* \to gg, \quad {q_i}^* \to q_i \gamma. \end{aligned} \tag{2}$$

For details, we refer the reader to Ref. [52]. We add that the gluon splitting in the above includes the splitting $g^* \to Q\bar{Q}$ where Q stands for heavy quarks (charm or bottom) if the virtuality is large enough to admit this process. We shall see later that this process plays an important role, which is likely to increase with the increasing center-of-mass energy of the collision. Because of the specifics of the implementation of the collision term in VNI/BMS, the reverse process, parton fusion, is not included, since it would lead to the propagation of partons off shell, which is not included in the VNI/BMS formulation. Technically, parton fusion with on-shell partons can be formulated via a $3 \to 2$ process that can be implemented using collision rates in the collision term. This has been successfully done in the BAMPS model [54]. The main drawback of the lack of parton fusion in VNI/BMS is that it violates detailed balance in the collision term and thus leads to an incorrect equilibrium

[1] The one exception is the BAMPS implementation [54].

[2] Historically, VNI/BMS is based on PYTHIA6 with the addition of a Boltzmann equation solver for the space-time evolution of all partons.

limit for the bulk in the infinite time and size limit. While this is a valid concern if we were to study the equilibration of bulk QCD matter in our approach, our focus on high-momentum heavy quarks that are not thought to thermalize fully [55] reduces the systematic uncertainty induced by the omission of these processes.

B. Heavy quark production by gluon fusion and annihilation of light quarks

At lowest order pQCD, heavy quarks are produced from fusion of gluons ($gg \to Q\bar{Q}$) and annihilation of light quarks ($q\bar{q} \to Q\bar{Q}$).

The partial differential cross section can be written as

$$\frac{d\hat{\sigma}}{d\hat{t}} = \frac{1}{16\pi\hat{s}^2}\sum|\mathcal{M}|^2, \tag{3}$$

where the summed spin- and colored-averaged squared matrix element for the process $gg \to Q\bar{Q}$ is given by

$$\sum|\mathcal{M}|^2 = \pi^2\alpha_s^2(Q^2)[a_1 + a_2 + a_3 + a_4 + a_5 + a_6], \tag{4}$$

where

$$\begin{aligned}
a_1 &= \frac{12}{\hat{s}^2}(M^2-\hat{t})(M^2-\hat{u}),\\
a_2 &= \frac{8}{3}\frac{(M^2-\hat{t})(M^2-\hat{u}) - 2M^2(M^2+\hat{t})}{(M^2-\hat{t})^2},\\
a_3 &= \frac{8}{3}\frac{(M^2-\hat{t})(M^2-\hat{u} - 2M^2(M^2+\hat{u})}{(M^2-\hat{u})^2},\\
a_4 &= -\frac{2M^2(\hat{s}-4M^2)}{3(M^2-\hat{t})(M^2-\hat{u})},\\
a_5 &= -6\frac{(M^2-\hat{t})(M^2-\hat{u}) + M^2(\hat{u}-\hat{t})}{\hat{s}(M^2-\hat{t})},\\
a_6 &= -6\frac{(M^2-\hat{t})(M^2-\hat{u}) + M^2(\hat{t}-\hat{u})}{\hat{s}(M^2-\hat{u})}.
\end{aligned} \tag{5}$$

The total cross section $\hat{\sigma}(\hat{s})$ is obtained from the above by integrating over $\hat{t}$:

$$\hat{\sigma}(\hat{s}) = \frac{1}{16\pi\hat{s}^2}\int_{M^2-\hat{s}(1+\chi)/2}^{M^2-\hat{s}(1-\chi)/2} d\hat{t}\sum|\mathcal{M}|^2, \tag{6}$$

where

$$\chi = \sqrt{1-\frac{4M^2}{\hat{s}}}. \tag{7}$$

We note that due to the mass of the heavy quark M this cross section remains finite and the total cross section reduces to

$$\begin{aligned}
\hat{\sigma}_{gg\to Q\bar{Q}}(\hat{s}) = \frac{\pi\alpha_s^2(Q^2)}{3\hat{s}}\Bigg[&-\left(7+\frac{31M^2}{\hat{s}}\right)\frac{1}{4}\chi\\
&+\left(1+\frac{4M^2}{\hat{s}}+\frac{M^4}{\hat{s}^2}\right)\log\frac{1+\chi}{1-\chi}\Bigg].
\end{aligned} \tag{8}$$

Similarly, the summed spin and coloured averaged squared matrix element for the process $q\bar{q} \to Q\bar{Q}$ is given by

$$\begin{aligned}
&\sum|\mathcal{M}|^2\\
&= \frac{64}{9}\pi^2\alpha_s^2(Q^2)\left[\frac{(M^2-\hat{t})^2+(M^2-\hat{u})^2+2M^2\hat{s}}{\hat{s}^2}\right],
\end{aligned} \tag{9}$$

so that the total cross section becomes.

$$\hat{\sigma}_{q\bar{q}\to Q\bar{Q}}(\hat{s}) = \frac{8\pi\alpha_s^2(Q^2)}{27\hat{s}^2}(\hat{s}+2M^2)\chi. \tag{10}$$

Once again, these cross sections remain finite due to the mass of the heavy quarks.

C. Heavy quark production due to flavour excitation

The implementation of heavy quark production due to flavor excitation has been subject of significant debate in the community. In principle, the (off-shell) heavy sea quarks in the target (projectile) can be brought on shell by scattering with other off-shell partons from the projectile (target) (or by scattering with on-shell partons that are produced during an earlier partonic interaction). This contribution was referred to as flavor excitation in the original paper of Combridge [56]. Its inclusion in the parton cascade model, where all parton scatter is treated at lowest order, has been questioned [37]. It is also seen to give rise to a substantial production of charm and bottom quarks [49], as was also pointed out in the original work of Combridge. It has been argued that this contribution should be strongly suppressed if higher order coherent interference terms are accounted for (see Ref. [57] and references therein).

In our calculation, we have excluded this process for the production of charm or bottom quarks. This is done in two steps. Firstly, we initialize the quark and gluon distribution functions at a rather low Q_0^2 of 0.589 GeV^2 (see Ref. [52]), which effectively eliminates the presence of heavy sea quarks. In addition, we disallow any partonic interaction if one of the partons is a heavy (charm or bottom) quark from the sea.

The flavor excitation process as it is understood now is included in next-to-leading-order (NLO) calculations, e.g., Refs. [38,39], and proceeds via a splitting of a gluon into a $Q\bar{Q}$ pair followed by scattering of one of the heavy quarks with another parton in the system. The contribution from this process to heavy quark production is not large. We re-emphasize that as mentioned earlier, the splitting of the final-state gluon into a charm-anticharm pair (or for that matter bottom-antibottom pair as well) is included in our calculations. We also add that soft collinear effective theory has been used recently to estimate the gluon splitting into heavy quarks [58], which suggests that this contribution can be large at LHC energies. Once produced, the heavy quarks are allowed to scatter with quarks and gluons. We shall see later that this plays an important role in their dynamics.

D. Scattering of light quarks and gluons with heavy quarks

We consider elastic scattering of heavy quarks with light quarks and gluons, i.e.,

$$Qq(\bar{q}) \to Qq(\bar{q}) \quad \text{and} \quad Qg \to Qg. \tag{11}$$

The differential scattering cross section is defined as

$$\frac{d\hat{\sigma}}{d\hat{t}} = \frac{1}{16\pi(\hat{s}-M^2)^2}\sum|\mathcal{M}|^2. \quad (12)$$

The summed spin- and colored-averaged squared matrix element for the process $Qq(\bar{q}) \to Qq(\bar{q})$ has been derived by Combridge [56]:

$$\sum|\mathcal{M}|^2 = \frac{64}{9}\pi^2\alpha_s^2(Q^2)\left[\frac{(M^2-\hat{u})^2+(\hat{s}-M^2)^2+2M^2\hat{t}}{\hat{t}^2}\right]. \quad (13)$$

The corresponding matrix element for the process $Qg \to Qg$ is given by

$$\sum|\mathcal{M}|^2 = \pi^2\alpha_s^2(Q^2)[b_1+b_2+b_3+b_4+b_5+b_6], \quad (14)$$

where

$$b_1 = 32\frac{(\hat{s}-M^2)(M^2-\hat{u})}{\hat{t}^2},$$
$$b_2 = \frac{64}{9}\frac{(\hat{s}-M^2)(M^2-\hat{u})+2M^2(\hat{s}+M^2)}{(\hat{s}-M^2)^2},$$
$$b_3 = \frac{64}{9}\frac{(\hat{s}-M^2)(M-\hat{u})+2M^2(M^2+\hat{u})}{(M^2-\hat{u})^2},$$
$$b_4 = \frac{16}{9}\frac{M^2(4M^2-\hat{t})}{(\hat{s}-M^2)(M^2-\hat{u})},$$
$$b_5 = 16\frac{(\hat{s}-M^2)(M^2-\hat{u})+M^2(\hat{s}-\hat{u})}{\hat{t}(\hat{s}-M^2)},$$
$$b_6 = -16\frac{(\hat{s}-M^2)(M^2-\hat{u})-M^2(\hat{s}-\hat{u})}{\hat{t}(M^2-\hat{u})}. \quad (15)$$

The total cross section is formally defined as

$$\hat{\sigma}_{\rm tot} = \frac{1}{16\pi(\hat{s}-M^2)^2}\int_{-(\hat{s}-M^2)^2/\hat{s}}^{0} d\hat{t}\sum|\mathcal{M}|^2. \quad (16)$$

We immediately note that the total cross sections for both the processes diverge because of the pole at $\hat{t}$ equal to zero. We reduce the upper limit of integration to $\hat{t} = -Q_0^2$, where $Q_0^2 = p_0^2$ and p_0 is the cutoff used in the parton cascade model, to regularize the $2 \to 2$ pQCD matrix element, as in PYTHIA.

E. Radiation of gluons by heavy quarks

The parton cascade model includes final-state radiation of gluons or photons following a hard ($2 \to 2$) scattering using the well-established approach of parton showers [59] as implemented in PYTHIA, in a leading logarithmic approximation. It incorporates a sequence of nearly collinear splittings, $a \to bc$, where the initial parton a is called mother parton and b and c are called daughters, which can split further and populate a treelike structure. Strong and electromagnetic interactions allow for several different possibilities of splittings, which are all included in the PCM. The differential probability for a splitting to occur is given by

$$\mathcal{P}_a = \sum_{b,c}\frac{\alpha_{abc}}{2\pi}P_{a\to bc}\frac{dQ^2}{Q^2}dz, \quad (17)$$

where the sum runs over all the allowed splittings and α_{abc} is equal to α_{em} for emission of photons and is α_s for QCD splittings. Further, Q^2 is the momentum scale of the splitting, z gives fraction of energy carried by the daughter b, and $1-z$ is the remaining fraction, carried by the daughter c. The kernels describing the splitting $P_{a\to bc}$ are taken from Altarelli and Parisi [60].

The parton cascade model uses a cutoff μ_0, taken as $\geqslant$1 GeV, to regulate the collinear singularities, by terminating the splitting once the virtuality of the timelike parton drops to μ_0. The soft gluon interference is accounted for by implementing an angular ordering of the radiated gluons. The mass of the partons is accounted for by modifying the cutoff μ_0 such that $\mu_0^2 = 1$ GeV^2 for gluons and $\mu_0^2 = m_q^2 + 1$ (GeV^2) for quarks [46] and thus radiation of gluons from heavy quarks is at the same footing as for that from light quarks. This value of μ_0 is same as that used in PYTHIA for regularizing the final-state (and initial-state) radiations. Increasing this will lead to a hardening of the transverse momentum spectra as well as a reduction in the number of collisions due to a reduction in number of gluons, while taking a smaller value would have an opposite effect. We shall see later that we get a reasonable description of the spectra for charm quarks both for pp and AA collisions and thus have kept it fixed, though exploratory calculations were done to verify the comments made above.

F. Production of heavy quarks using the minijet formalism

In order to validate the Monte Carlo implementation of the PCM that we are using, we perform a separate calculation of heavy quark production using the minijet formalism [61]. The cross section for the production of a heavy-quark pair ($Q\bar{Q}$) is written in terms of the rapidities of the two quarks y_1 and y_2 and their transverse momentum p_T as

$$\frac{d\sigma}{dp_T^2 dy_1 dy_2} = \sum_{ij}\frac{1}{1+\delta_{ij}}\Big[x_a f_i^{(a)}(x_a,Q^2)x_b \times f_j^{(b)}(x_b,Q^2)\frac{d\hat{\sigma}_{ij}}{d\hat{t}}(\hat{s},\hat{t},\hat{u})x_a f_j^{(a)}(x_a,Q^2)x_b \times f_i^{(b)}(x_b,Q^2)\frac{d\hat{\sigma}_{ij}}{d\hat{t}}(\hat{s},\hat{u},\hat{t})\Big]. \quad (18)$$

In the above, $f_i^{(a)}$ denotes structure function of the parton i for the nucleon a, etc., x_a is the fraction of linear momentum of the nucleon a carried by the parton, and Q^2 is the momentum scale, in the standard notation. However, in order to be able to directly compare it to the parton cascade model, we fix the fragmentation scale at the momentum cutoff p_0^2 used in the calculation for the momentum cutoff and the coupling constant is kept at a fixed value of α_s.

III. RESULTS

We shall first discuss our results for pp collisions at $\sqrt{s_{NN}} = 200$ GeV for several different parton interaction scenarios. Next we give our findings for Au + Au collisions at the same center-of-mass energy for central collisions. Finally we compare the proton-proton results to the Au+Au results to

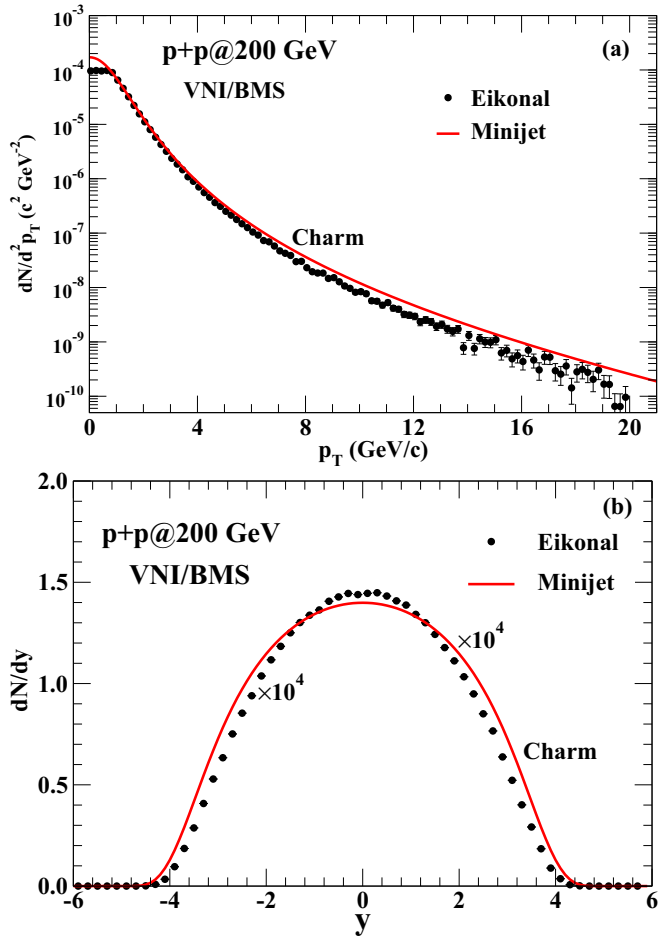

FIG. 1. (a) The rapidity (y) integrated p_T spectra of charm quarks using minijet calculations (solid curves) and eikonal approximation. The lower panel (b) gives the p_T integrated rapidity spectra.

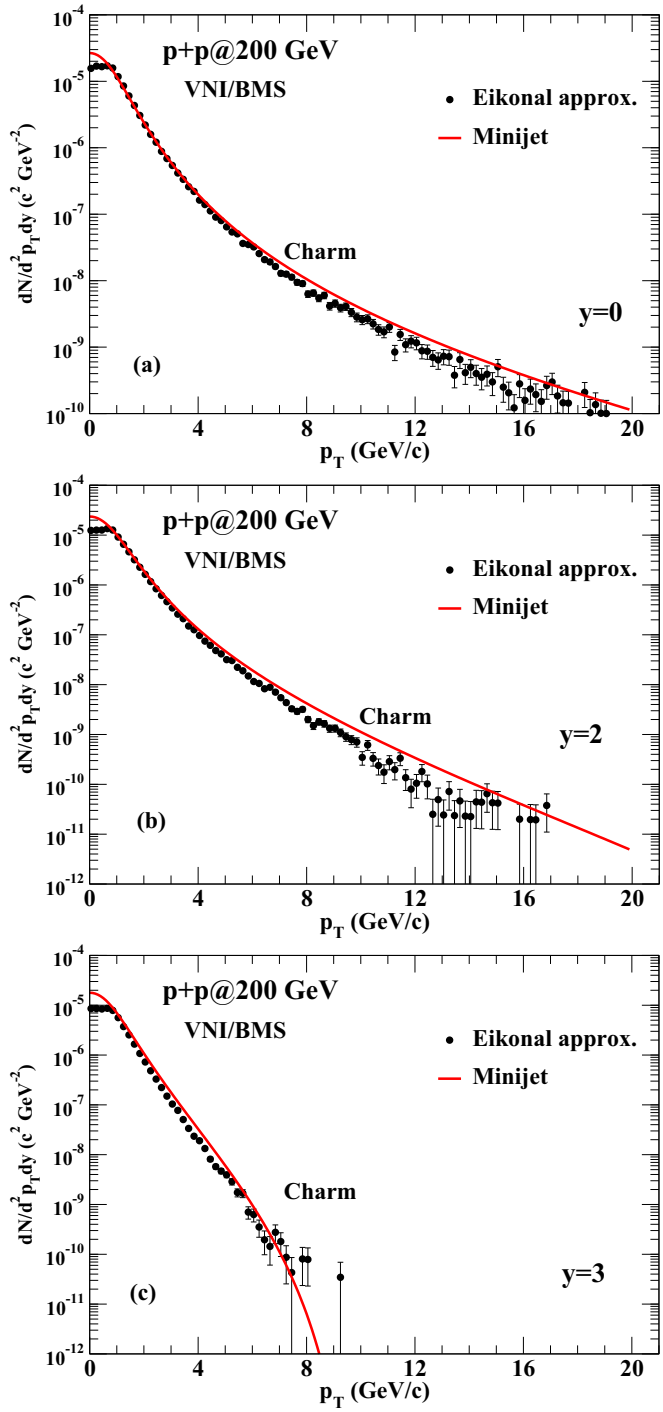

FIG. 2. The p_T spectra for charm quarks using minijet calculations (solid curves) and eikonal approximation at $y = 0$ (a), $y = 2$ (b), and $y = 3$ (c).

get an idea about the emerging dynamics of the propagation of charm quarks, subject to semihard scatterings and radiation of gluons in the QCD medium produced by relativistic heavy ion collisions.

A. *pp* collisions at $\sqrt{s_{NN}} = 200$ GeV

In order to test the accuracy of our implementation of heavy quark production in VNI/BMS, we first study collisions of protons at $\sqrt{s_{NN}} = 200$ GeV.

We calculate the production of charm quarks due to $gg \to Q\bar{Q}$ and $q\bar{q} \to Q\bar{Q}$ processes using a minijet calculation with a GRV-HO parametrization [62] of the parton distribution function. In order to compare it with our implementation of the PCM, we fix α_s as 0.3 and keep Q_0^2 fixed at 0.589 GeV^2 for the renormalization and factorization scales. Note that for a pure theory-to-theory comparison, the specifics of the parton distribution function are not of particular importance, which is why we choose the well established (even though somewhat dated) GRV-HO parametrization.

The minijet calculation is compared to a VNI/BMS calculation using an eikonal approximation, where the final momenta and flavors of the particles produced in a hard scattering are replaced by the momenta and flavors of the corresponding initial-state partons. This procedure thus mimics the eikonal approximation. A comparison of these two calculations can be found in Figs. 1 and 2: The rapidity integrated transverse momentum spectrum and the p_T integrated rapidity spectrum of the produced charm (or anticharm) are given in Fig. 1 and the p_T spectra at several rapidities are given in Fig. 2. We observe

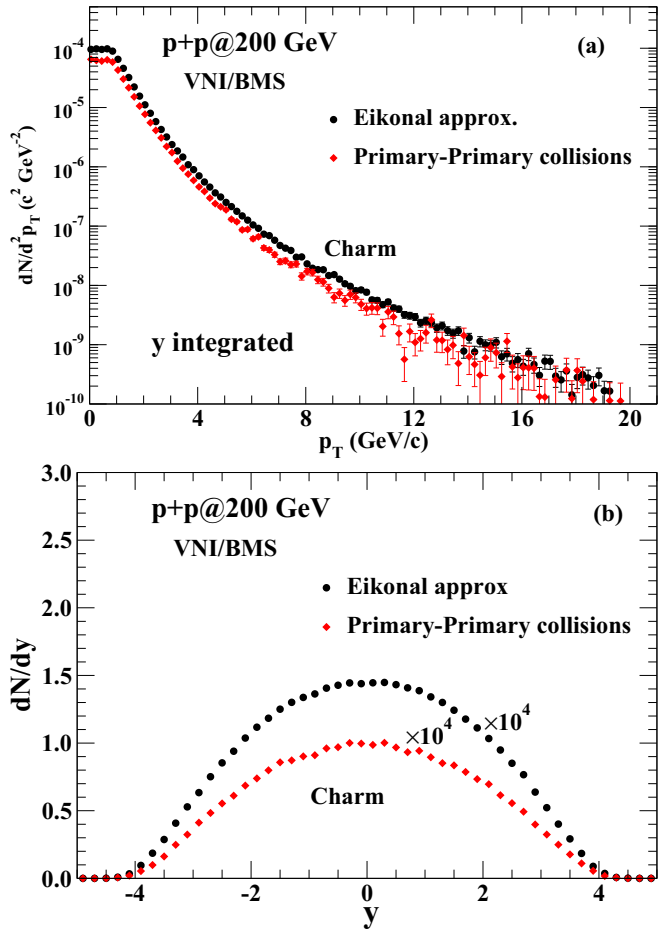

FIG. 3. (a) The rapidity integrated p_T spectra and (b) p_T integrated rapidity spectra for charm quarks using eikonal approximation and primary-primary collisions for pp system at $\sqrt{s_{NN}} = 200$ GeV.

satisfactory agreement between the VNI/BMS calculation and the minijet reference. The minor differences at very low and very high p_T arise due to the p_T cutoff in the parton cascade model, which is also reflected in $x_{\min}$ which enters in the parton cascade model. This difference is again reflected in the rapidity distribution as well.

Having established reasonable quantitative agreement between the two independent calculations and thus confirming that heavy quark interactions are correctly implemented in the Monte Carlo scheme of VNI/BMS, we proceed to study the dynamics of the cascade evolution. As a first step, we consider a calculation in which only primary-primary parton interactions are permitted; i.e., each parton is allowed to interact only once. A comparison of these calculations with the results of the eikonal approximation then immediately highlights the effect of multiple parton interactions in the eikonal approximation, already in pp collisions. Again we show the rapidity integrated transverse momentum spectrum and the p_T integrated rapidity spectrum of the produced charm (or anticharm) in Fig. 3. The spectra are quite similar in shape but differ by the factor which accounts for the increased number of collisions in the eikonal approximation. Details of the evolution of the cascade are quantified in Table I. We see from Table I that the leading process which contributes to the production of charm quarks, i.e., $gg \to c\bar{c}$, is about 50% more likely in the eikonal approximation compared to the case when only primary-primary collisions are allowed.

Now we proceed to results with the proper accounting of multiple scatterings along with the changes in the flavor and momenta of the produced partons, before they scatter again. These studies, we believe, will help us identify the effects of multiple scatterings already at the level of $p + p$ collisions.

Looking at Table I, we find there is an increase in the number of collisions by about 20% compared to the eikonal approximation. Compared to the primary-primary collision calculation, the increase is about 60%. While the increase in the number of collisions for the case of multiple scatterings over and above that of the case of primary-primary collisions is expected, the increase in the number of collisions above that for the eikonal approximation comes as a surprise. This may be due to interactions that impart a large momentum to partons that previously would have been below the momentum cutoff for an interaction now acquiring sufficient transverse momentum for subsequent interactions.

The rapidity integrated p_T and the p_T integrated rapidity spectra are shown in Fig. 4. We see that a proper accounting of the changing momenta and the flavors of the partons following a hard scattering enhances the production of charm quarks at moderate transverse momenta. This effect will undoubtedly be even more prominent in Au + Au collisions, where the probability of multiple scatterings increases considerably. However, there are already indications of nonuniform variation of the factor by which the two calculations differ as a function of p_T and y, presumably due to the larger density of interacting partons at midrapidity.

Finally, we include timelike branchings of partons in our calculation, which leads to a rapid increase in the number of partons at midrapidity and subsequent multiple scatterings. As expected, we observe a considerable increase in the number of hard collisions, fueled by the timelike branchings which leads (mainly) to gluon multiplication. Once again we notice that the increase in $gg \to q\bar{q}$ is reflected in the increase of the production of charm quarks. This close correspondence may be due to fact that the medium generated in pp collisions is not yet dense and long lived enough to have several scatterings by partons which can reduce their momenta such that further collisions do not produce heavy quarks. The momenta of charm quarks at medium and large p_T are also greatly affected (see Fig. 5) while a comparison of the rapidity distribution suggests increased interactions at central rapidities (Fig. 5).

Even though not substantial, we also observe perceptible change in the momentum distribution obtained in eikonal approximation compared to the case for proper multiple collisions, as these actually evolve. This would imply a slight correction to the standard calculations for the proton-proton baseline for the medium modification of particle production if estimated within the eikonal approximation. However, one would require very high-precision data to quantitatively investigate this effect.

Charm production in pp collisions has been measured by the STAR experiment [63] by measuring D^0 production and other D mesons. We can compare our results for the

TABLE I. The number of scatterings and timelike branchings involving different subprocesses in pp collisions at $\sqrt{s_{NN}} = 200$ GeV.

Process	Only primary-primary collisions	Eikonal approximation	Multiple collisions	Multiple collisions and radiation
$q + q \to q + q$	0.204	0.255	0.269	0.364
$q + \bar{q} \to q + \bar{q}$	0.002	0.002	0.002	0.012
$q + \bar{q} \to g + g$	0.006	0.008	0.008	0.032
$q + \bar{q} \to g + \gamma$	0.0	0.0	0.0	0.0
$q + \bar{q} \to 2\,\gamma$	0.0	0.0	0.0	0.0
$q + g \to q + g$	1.062	1.447	1.617	2.874
$q + g \to q + \gamma$	0.0	0.001	0.001	0.004
$g + g \to q + \bar{q}$	0.008	0.011	0.014	0.052
$g + g \to g + g$	0.985	1.533	1.852	4.814
Total hard $a + b \to c + d$	2.267	3.257	3.764	8.152
$q \to q + g$				0.710
$g \to g + g$				2.989
$g \to q + \bar{q}$				0.255
$q \to q + \gamma$				0.0
Total $a \to b + c$				3.954
N_c $(=\bar{N}_c)$/event	4.98×10^{-4}	7.62×10^{-4}	9.08×10^{-4}	34.95×10^{-4}

distribution of charm quarks by accounting for the fragmentation ratio (≈0.565) for the $c \to D^0$ fragmentation as also in the above reference for a comparison results from with PYTHIA (tuned) and FONLL calculations. This amounts to assuming that the fragmentation function varies as $\delta(1 - z)$ (see later). Our results for the calculations incorporating multiple scattering

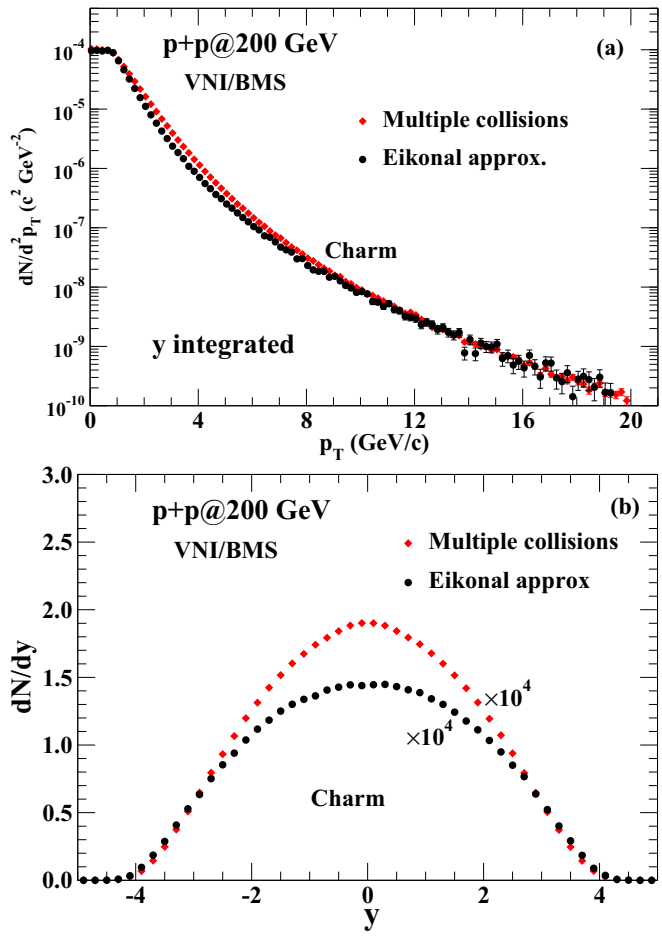

FIG. 4. (a) The rapidity integrated p_T spectra and (b) p_T integrated rapidity spectra for charm quarks using eikonal approximation and multiple collisions for pp system at $\sqrt{s_{NN}} = 200$ GeV.

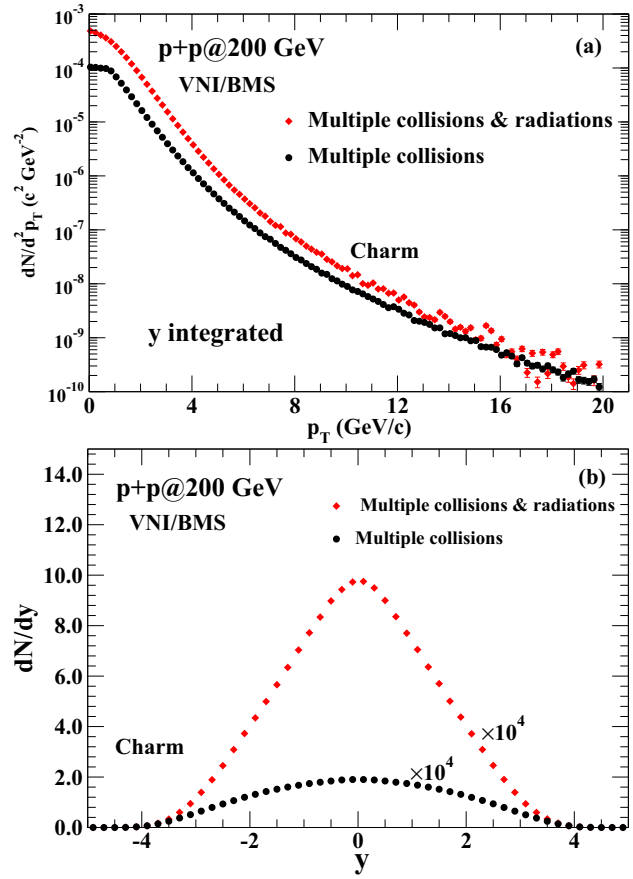

FIG. 5. (a) The rapidity integrated p_T spectra and (b) p_T integrated rapidity spectra for charm quarks using multiple collisions only and multiple collisions as well as fragmentation of partons scattered off the final-state partons, following a semihard scattering in evolution of the cascade for pp system at $\sqrt{s_{NN}} = 200$ GeV.

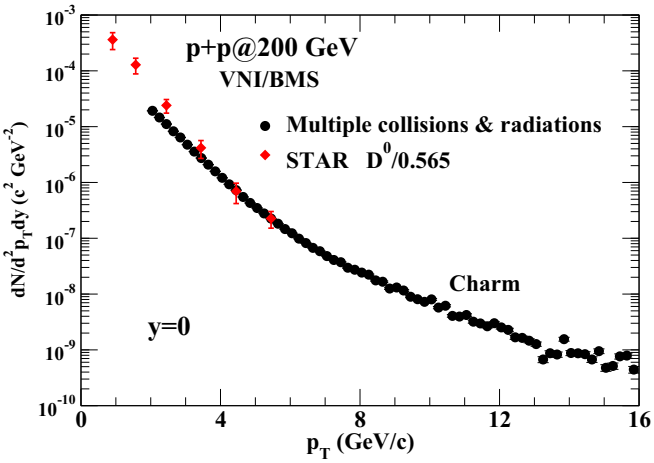

FIG. 6. The p_T spectra for charm quarks using multiple collisions as well as fragmentation of partons scattered off the final-state partons, following a semihard scattering in evolution of the cascade for pp system at $\sqrt{s_{NN}} = 200$ GeV. The data are from the STAR experiment [63].

and radiations are shown in Fig. 6. In view of the $p_T^{\text{cut-off}}$ and μ_0 used to regularize the matrix elements and fragmentation functions used in our work, we show the results for our calculations only for $p_T \geqslant 2$ GeV. A fair agreement is seen without any attempt to adjust any parameters.

B. Au + Au collisions at $\sqrt{s_{NN}} = 200$ GeV

When and where are most of the charm quarks produced in a nucleus-nucleus collision? How often do they undergo collisions? How often do they radiate gluons? How does the charm production depend on gluon multiplication? These and many other interesting details of charm production are easily discernible in the space-time description of the cascading partons in our calculations. We proceed to address these questions in the following sections.

1. Dynamics of charm production in cascading partons

We start by calculating the spatial distribution of the production vertices of the charm quarks along the beam axis (Fig. 7) for the different interaction scenarios introduced in the previous section. We see that for all cases studied (primary interactions only, secondary rescattering, and rescattering plus radiation) the production of charm quarks is symmetrically concentrated around the region of complete overlap ($z = 0$). We further note that charm-quark production is mostly limited to the zone around ± 0.5 fm along the beam axis, due to the Lorentz contraction of the colliding nuclei.

Focusing on the case where multiple collisions along with the fragmentation of partons is permitted, we note that the number of produced charm quarks is significantly larger than in the other cases. However, the fraction of charm quarks produced at later separations is now much smaller than that for the case when only multiple scatterings are permitted (see Fig. 7). Multiple collisions occur predominantly in the region of complete overlap. The colliding partons radiate gluons

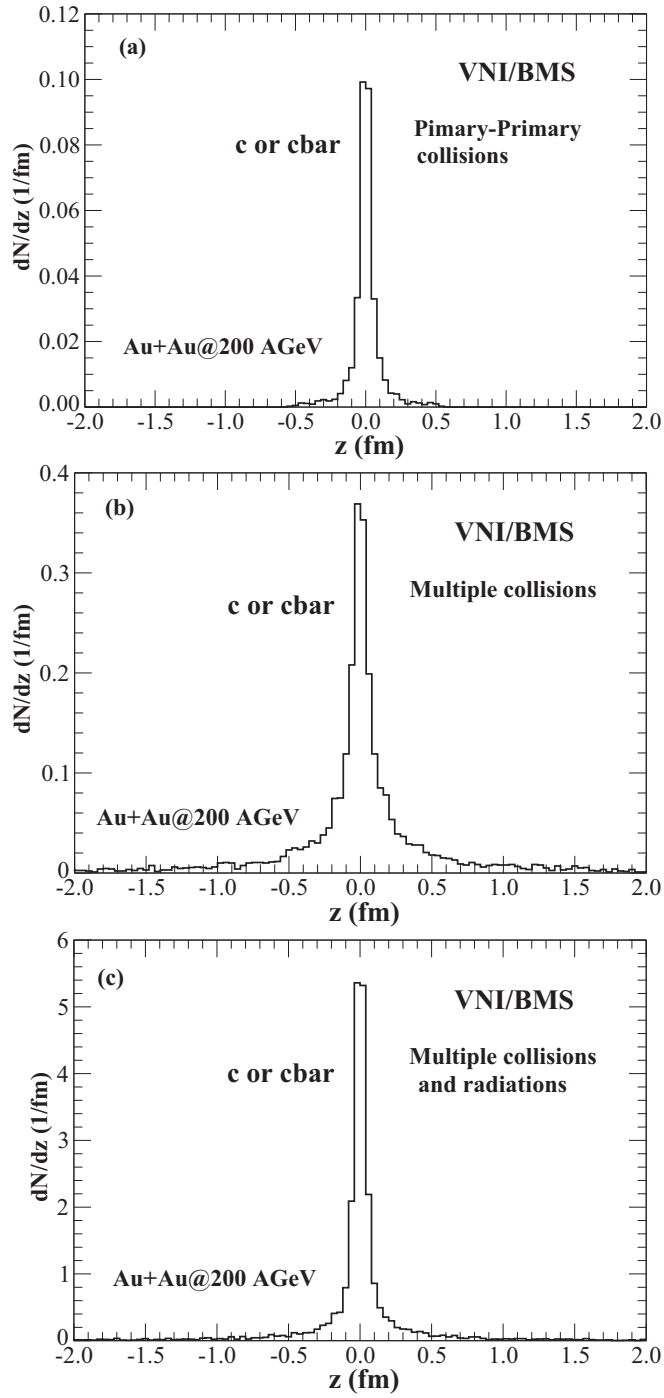

FIG. 7. The distribution of z coordinates of production vertices of charm (or anticharm) quarks for the cases involving only primary-primary collisions (a), only multiple collisions (b), and multiple collisions and radiations of gluons (c).

and rapidly lose energy, while the parton clouds continue to propagate through each other. However, by the time the gluons undergo third or fourth interaction, their energy has dropped significantly and subsequent interactions may not have enough energy to produce heavy quarks. On the other hand, if the partons were not allowed to radiate gluons as in the case of

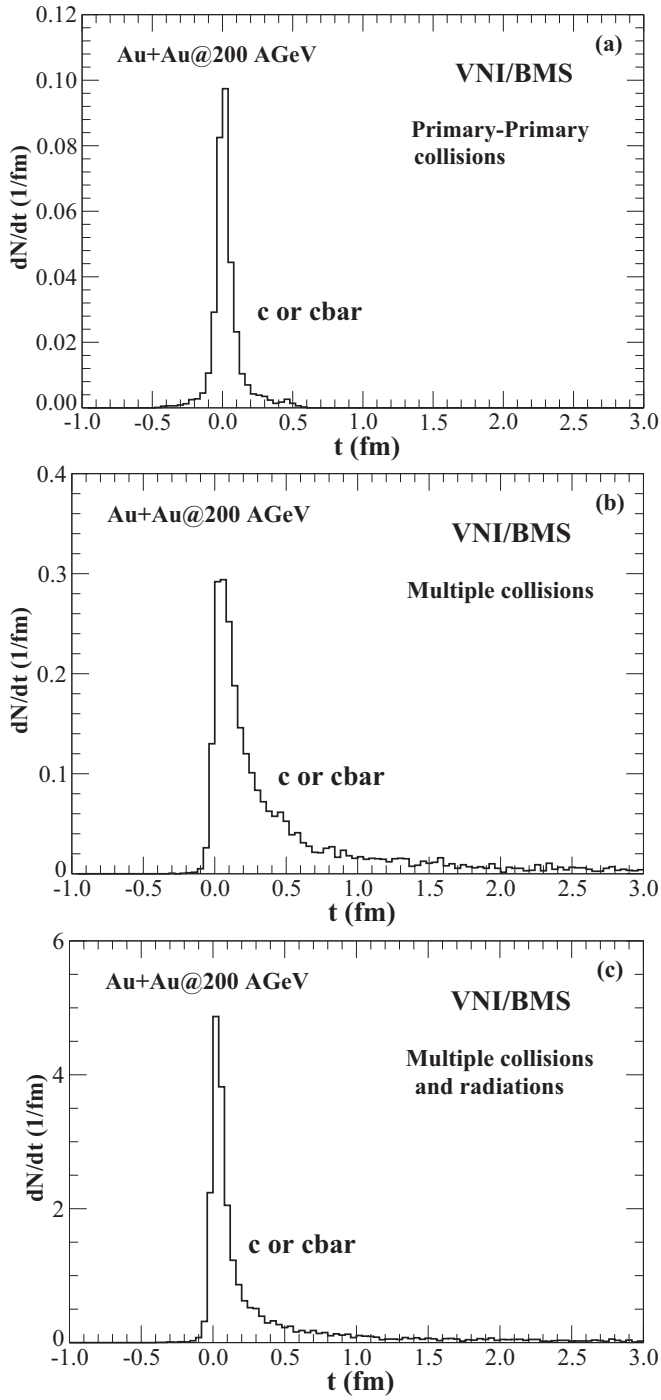

FIG. 8. The distribution of production times of charm (or anticharm) quarks for the cases involving only primary-primary collisions (a), only multiple collisions (b), and multiple collisions and radiations of gluons (c). Note that $t = 0$ is defined to occur when the two nuclei are in full overlap.

multiple scatterings without radiations, even the later collisions have enough energy to produce heavy quarks. This scenario is further reinforced by the observations of Fig. 8, which shows the distribution of the production times of charm quarks.

Charm production generally commences by the time the nuclei start touching other, increases rapidly as they interpenetrate, peaks when they are on top of each other, and falls off as the nuclei disengage. A similar trend is seen in the behavior of the z distribution of the production vertices. When the multiple scatterings are permitted (without radiations), the production of charm quarks continues (albeit at a very small rate) until almost 3 fm/c after the complete overlap of the nuclei, though most of them are produced by about 0.5–1.0 fm/c. For the last case, when the radiation of gluons is permitted, a rapid multiplication of partons and a considerable increase in multiple scatterings is observed. As a consequence, there is a large increase in production of charm quarks as well. However, this additional production is now mostly limited to early times, say about 0.3–0.5 fm/c. We attribute this restriction to early times to the energy lost by partons due to radiation of gluons following multiple scatterings: collisions at later times involve energies which are below the threshold for production of charm. We emphasize, however, that even though the production of charm quarks is essentially over by about 0.5 fm/c the collisions (and radiations) will continue until about 3–4 fm/c and thus charm quarks (and other high-energy quarks or gluons) will continue to lose energy due to semihard processes [52].

In Fig. 9, we show the actual distribution of t and z positions of the production vertices (for about 2700 charm quarks) for the three cases discussed above. We notice that the t and z coordinates of the production vertices for the primary-primary collision case are located close to the world lines describing the motion of the centers of the two nuclei and are limited to the time of overlap. For the case of multiple collisions only, the production continues to late times and fills up larger distances from the point of complete overlap. For the case when both multiple scatterings and radiation (of gluons) are permitted, we have a concentration of production vertices around the time of overlap, as at later times the partons do not have enough energy to cross the threshold for the production of charm-anticharm pairs. The corresponding x and y coordinates for the three cases are shown in Fig. 10. We have verified that these distributions closely follow the distribution of binary collisions $n_{\mathrm{BC}}(x, y)$ obtained using a Glauber model [5].

How often do the charm quarks scatter after production and how often do they radiate gluons? The distribution of the number of scatterings suffered by charm quarks for the two cases that allow rescattering after production is given in Fig. 11. The produced charm quarks, being secondary particles, will not scatter when only primary-primary parton interactions are considered. We also show the distribution of the number of gluon splittings by the charm quarks (Fig. 12) for the case when we consider both multiple scattering and multiplication of gluons due to their radiation off scattered partons.

When only multiple scatterings are permitted, charm quarks will rarely scatter more than 3–4 times. We attribute this limitation to the number of partons remaining limited and thus the possibility of an interaction decreasing rapidly as the parton clouds disengage. However, when the fragmentation of final-state partons produced in a hard scattering is allowed, the number of gluons increases rapidly and leads to a significantly larger number of scatterings and a significant production of gluons due to radiation. Now we find that charm quarks may scatter up to 20 times, with 8–10 scatterings not being too

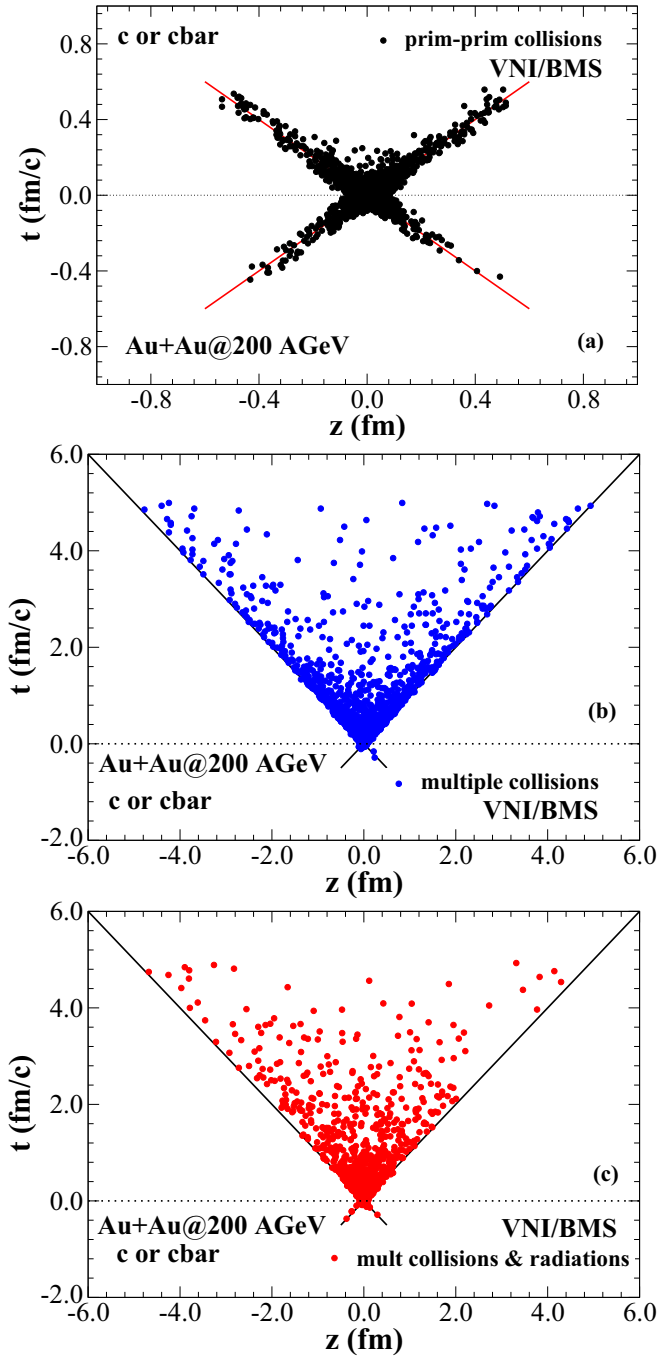

FIG. 9. The z and t coordinates of production vertices of charm (or anticharm) quarks for the cases involving only primary-primary collisions (a), only multiple collisions (b), and multiple collisions and radiations of gluons (c). Note the change of scale along the z axis for the primary-primary case.

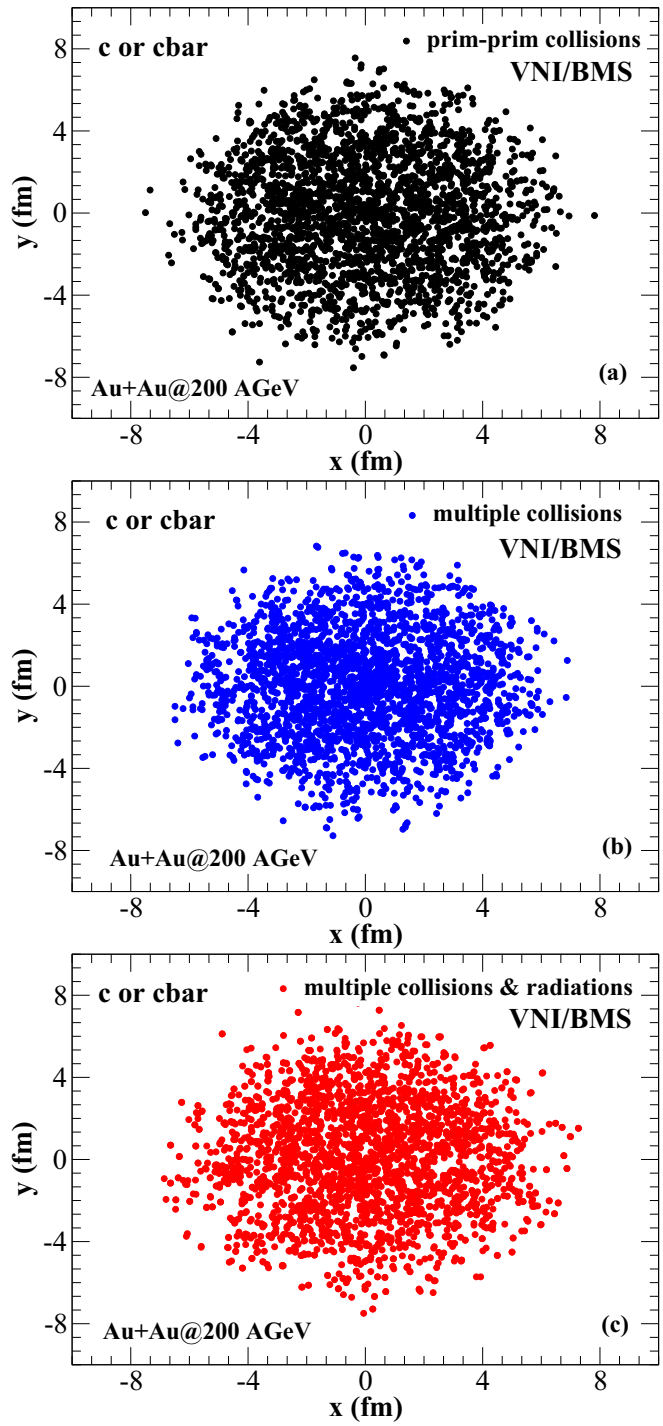

FIG. 10. The x and y coordinates of production vertices of charm (or anticharm) quarks for the cases involving only primary-primary collisions (a), only multiple collisions (b), and multiple collisions and radiations of gluons (c).

uncommon. Despite the restriction of the PCM to interactions above a p_T cutoff, this large number of semihard scatterings has the potential to start propelling charm quarks toward thermalization!

Finally in Fig. 12 we provide results for the occurrences of the splitting of gluons off charm quarks following a semihard scattering (note that we only count the number of initial splittings, not the total number of gluons that may be emitted in each of these processes). While one splitting is most frequent, we do observe some occurrences of multiple splittings.

Table II provides a quantitative summary of the above analysis. For example, we find that total number of semihard

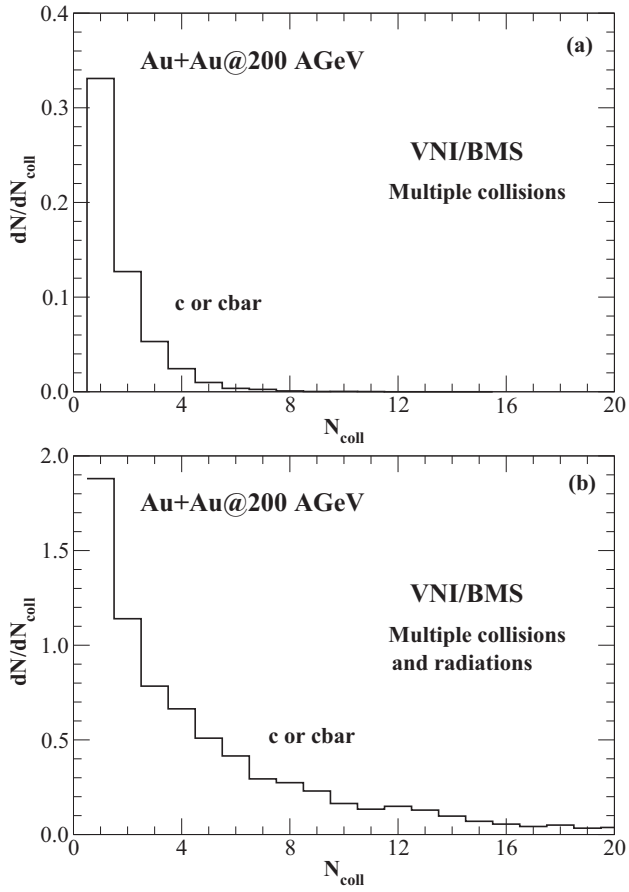

FIG. 11. (a) The distribution of number of collisions encountered by charm quarks when only multiple scattering among partons is permitted and (b) when both multiple scattering and radiations are permitted.

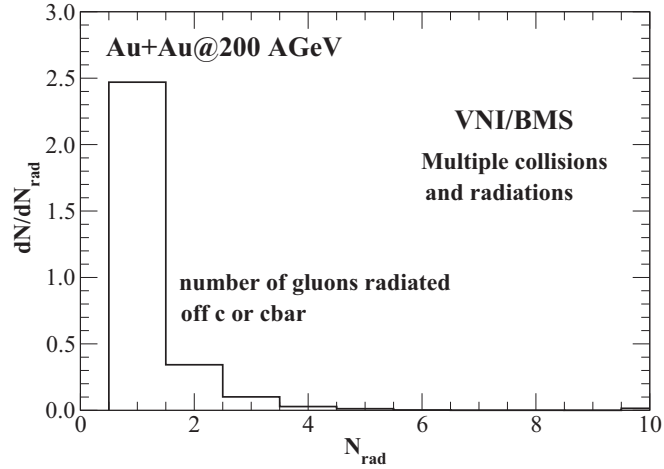

FIG. 12. The distribution of number of gluons radiated off charm quarks following a semihard scattering.

scatterings for all partons increases by a factor of 2.2 when we perform calculations in the eikonal approximation, a factor of about 3.5 when we perform the calculation using multiple scatterings, and a factor of about 19 when we perform calculations allowing for multiple scatterings and multiplication of partons due to timelike branchings or fragmentations—in comparison to the calculation involving only primary-primary interactions. The number of collisions for the leading process for charm production included in the counting of, $gg \to q\bar{q}$, rises by factors of 2.2, 4.3, and 44, respectively.

The production of charm quarks shows increases by factors of 2.5, 4, and 15.2 respectively. We note that while the rise in charm production in going from primary-primary scatterings to the eikonal approximation to multiple scatterings closely follows the trend for the rise in the $gg \to q\bar{q}$ process, the rise in charm production when we consider multiple scatterings with parton multiplications is much less (only a factor of about 15) compared to the rise in such processes (about a factor of 44) for light parton interactions. As discussed previously, we attribute this reduced increase to gluon multiplication leading to an ensemble of less energetic partons so that despite the increase

TABLE II. The number of scatterings and timelike branchings involving different subprocesses in Au + Au collisions at 200 A GeV.

Process	Only primary-primary collisions	Eikonal approximation	Multiple collisions	Multiple collisions and radiation
$q + q \to q + q$	111.2	185.3	227.8	591.5
$q + \bar{q} \to q + \bar{q}$	1.1	1.4	2.2	34.0
$q + \bar{q} \to g + g$	3.7	5.4	7.6	86.7
$q + \bar{q} \to g + \gamma$	0.0	0.1	0.0	0.8
$q + \bar{q} \to 2\,\gamma$	0.0	0.0	0.0	0.0
$q + g \to q + g$	527.7	1056.9	1538.3	6370.0
$q + g \to q + \gamma$	0.3	0.4	0.7	11.8
$g + g \to q + \bar{q}$	3.7	8.0	16.3	164.8
$g + g \to g + g$	432.7	1109.8	2020.6	13304.0
Total hard $a + b \to c + d$	1080.6	2367.3	3813.4	20563.7
$q \to q + g$				787.0
$g \to g + g$				3868.2
$g \to q + \bar{q}$				345.5
$q \to q + \gamma$				0.0
Total $a \to b + c$				5000.8
N_c $(=\bar{N}_c)$/event	0.33	0.82	1.33	5.21

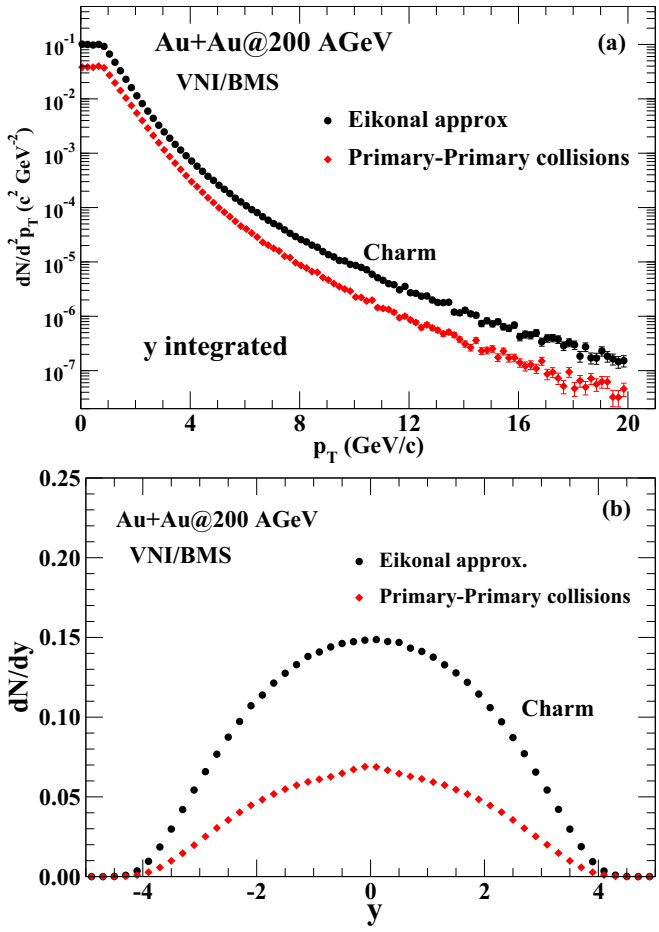

FIG. 13. (a) The y-integrated p_T spectra of charm quarks using eikonal approximation and only primary-primary collisions for the Au + Au system at $\sqrt{s_{NN}} = 200$ GeV. The lower panel (b) gives the p_T integrated rapidity spectra for the same cases.

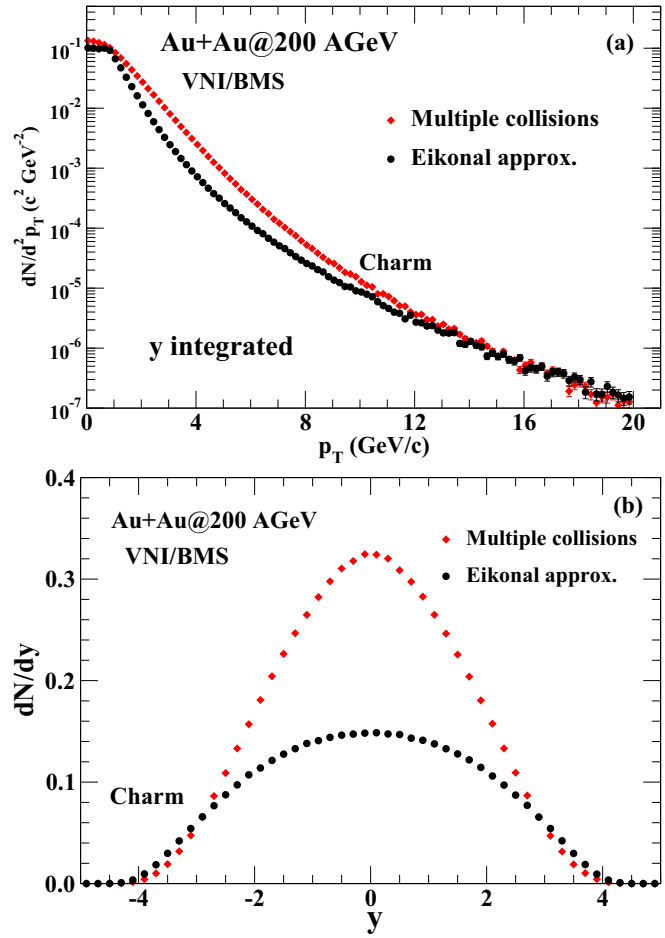

FIG. 14. (a) The y-integrated p_T spectra of charm quarks using eikonal approximation and multiple collisions for the Au + Au system at $\sqrt{s_{NN}} = 200$ GeV in parton cascade model. The lower panel (b) gives the p_T-integrated rapidity spectra for the same cases.

in the number of multiple collisions that partons suffer, they may not be energetic enough for the production of charm in later interactions.

2. *Spectra of charm quarks in Au + Au collision at $\sqrt{s_{NN}} = 200$ GeV*

In this section, we proceed to discuss our results for spectra of charm quarks produced in central collisions for Au + Au at $\sqrt{s_{NN}} = 200$ GeV, again using the same set of interaction models as in the previous section.

As a first step, we compare our results for the implementations of the eikonal approximation with those for primary-primary collisions (Fig. 13). We find that p_T spectra are similar but not identical in shape and differ by factors of 2–5 varying with p_T and also y.

The results for a comparison of the multiple scattering to that of the eikonal approximation are shown in Fig. 14. The p_T spectra for both calculations are quite similar for large p_T. However, we observe considerable differences at intermediate transverse momenta: While the results for the eikonal approximation mimic a power law, those for the case of multiple scattering exhibit more of an exponential shape. This is a consequence of multiple scatterings altering the parton momenta, which are properly accounted for in the parton cascade model. This observation is also supported by estimates of the production of charm quarks due to multiple scatterings among partons produced in semihard (mini)jets by several authors [23,36,37]. We note that the production of charm is proportionately higher at central rapidities as compared to larger rapidities in the case of multiple scattering.

Now we study the effect of gluon splitting on the charm spectra: For this purpose, we compare results for the production of charm quarks in the multiple scattering mode to that in which multiple scatterings as well as fragmentation of partons is enabled (Fig. 15). We observe a substantially larger production of charm at lower p_T and a suppressed production of charm at larger p_T. The increase in the production of charm at lower p_T is a consequence of the large increase in the population of low-momentum partons due to gluon multiplication. In addition, high-momentum charm quarks loose energy via gluon splitting and multiple scatterings with lower momentum partons.

The rapidity distribution of charm shows an enhanced production at central rapidities: While the overall increase

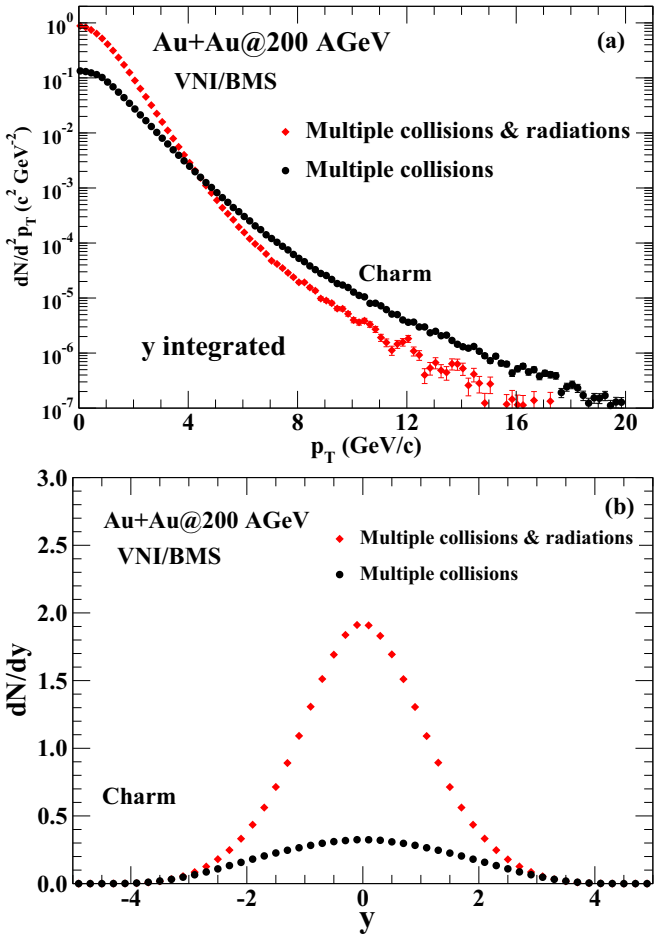

FIG. 15. (a) The y-integrated p_T spectra of charm quarks using multiple collisions and multiple collisions and fragmentations for Au + Au system at $\sqrt{s_{NN}} = 200$ GeV in parton cascade model. The lower panel (b) gives the p_T-integrated rapidity spectra for the same cases.

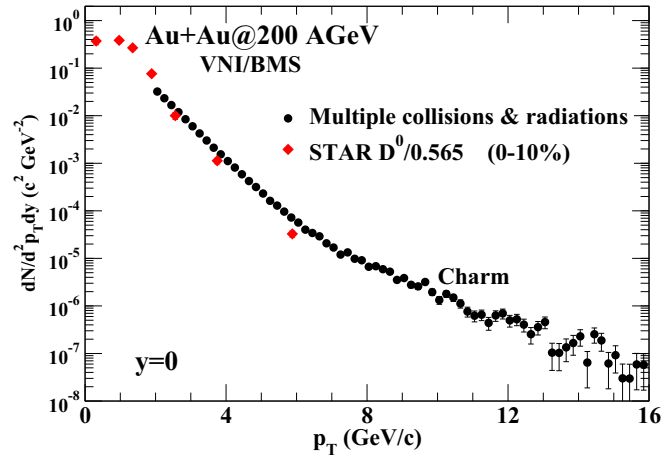

FIG. 16. The p_T spectrum of charm quarks at central rapidity along with the spectrum of D mesons obtained with STAR Collaboration [64] for the most central collisions for Au + Au system at $\sqrt{s_{NN}} = 200$ GeV. The parton cascade calculation includes multiple scatterings as well as radiations of gluons off final-state partons in semihard scatterings.

in production of charm is by a factor of about four, at central rapidity the rise is by a factor of six.

Comparing data on final-state hadrons, such as D mesons, to the PCM is inherently challenging, due to the limitation of the PCM to parton scattering above a momentum cutoff $p_T^{\min}$ as well as due to the systematic uncertainties inherent in the modeling of hadronization. A realistic hadronization model, accounting for bulk hadronization, parton recombination, and hadronization via fragmentation, is currently out of reach for this particular PCM implementation. Nevertheless, we shall attempt a series of schematic comparisons, by assuming a simple hadronization scheme for D mesons, based solely on the fragmentation of c quarks. Starting with a fragmentation function for the production of D mesons from charm quarks as $\delta(1-z)$, where z is the fraction of momentum of the charm quark carried by the D meson, we can assume that the p_T of the D mesons will be very similar to the p_T of the charm quarks themselves. This ansatz has widely been used in the literature (see, e.g., Refs. [66,67]). Please note, however, that more accurate fragmentation functions would show a narrow peak around the ratio of the masses of the charm quark and D mesons M_c/M_D (Ref. [68]). With this in mind, we compare the results of our calculations for the p_T spectrum of charm quarks at central rapidity, with the results for D^0 mesons obtained by the STAR Collaboration [64] for the most central collisions (Fig. 16) after adjusting it for the fragmentation ratio for the $c \to D^0$ fragmentation. We show our results only for $p_T > 2$ GeV, since our calculations do not include hydrodynamic flow, which is known to modify the spectra at lower transverse momenta, and we have used a $p_T^{\text{cut-off}}$ and μ_0 to regularize the pQCD matrices and $P_{a\to c}$ fragmentations. We see that the shape for the calculated spectrum is quite similar to the experimental result above a p_T of 2–3 GeV, where fragmentation should start to significantly contribute to charm quark hadronization. We do add that while our calculations are for zero impact parameter, the experimental data are for 0–10% central collisions, which have about a 10% smaller number of collisions.

3. *Nuclear modification factor for charm production*

The nuclear modification factor is defined by

$$R_{\text{AA}} = \frac{dN_{\text{AA}}/dp_T dy}{N_{\text{coll}} \times dN_{\text{pp}}/dp_T dy}, \tag{19}$$

where N_{coll} is the number of binary nucleon-nucleon collisions for a given centrality. R_{AA} is a measure of modification of the production processes due to the presence of the medium produced in the wake of the nucleus-nucleus collisions and has been used extensively to study the phenomenon of jet quenching.

As a first step, we compare calculations for the rapidity integrated R_{AA} for different interaction assumptions (Fig. 17). Unsurprisingly, we find that the results for the eikonal approximation are consistent with one, as one would expect from these calculations. The results for multiple scattering suggests a considerable increase in the production of charm

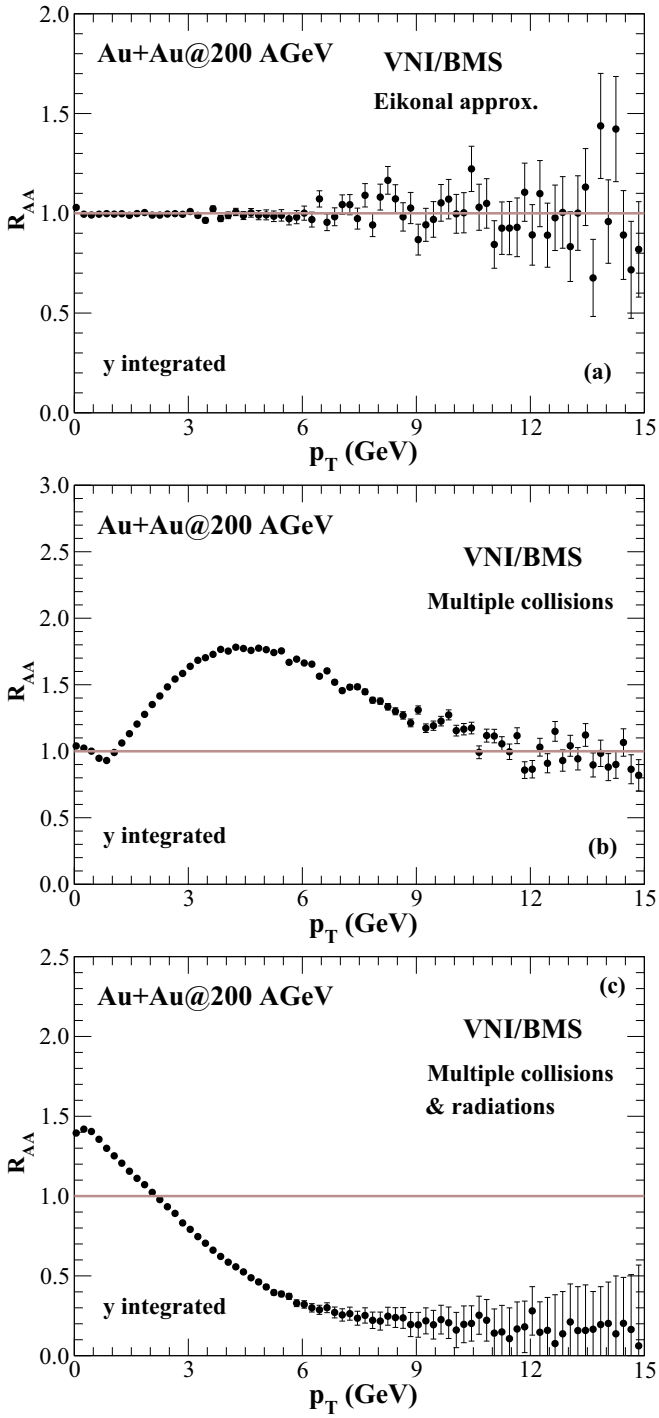

FIG. 17. Rapidity-integrated nuclear modification factor for eikonal approximation (a), multiple collisions (b), and multiple collisions along with the parton multiplications (c) for central collisions for Au + Au system at $\sqrt{s_{NN}} = 200$ GeV.

quarks at intermediate p_T beyond that which one would have expected on the basis of a mere superposition of pp collisions and is consistent with our findings discussed in previous sections.

The results for the full calculation, including multiple scatterings as well as parton fragmentations (mostly radiation

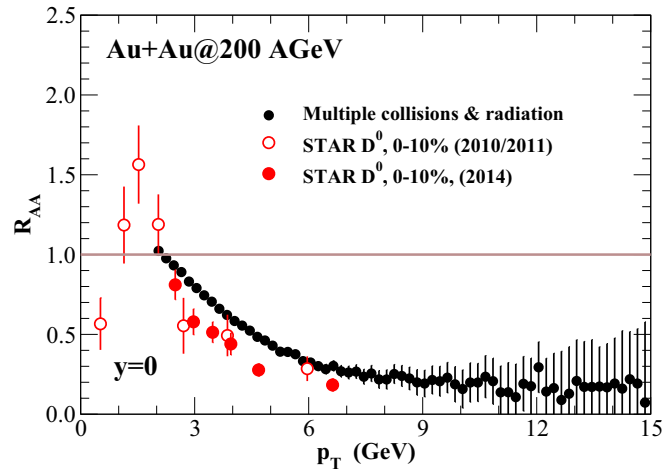

FIG. 18. Nuclear modification factor for central rapidity in the parton cascade model using multiple collisions along with the parton multiplications for central collisions for the Au + Au system at $\sqrt{s_{NN}} = 200$ GeV. The experimental data (with only statistical errors) are from the STAR Collaboration [64,65].

of gluons), provide some interesting findings: In the low-p_T domain, we observe an enhancement of charm production of more than 50% beyond what one would expect from mere superposition of pp collisions. Noting that the p_T of charm quarks can get strongly affected by hydrodynamic flow [69], these results are expected to change if a more realistic bulk medium evolution is included in the calculation. At large p_T we see a substantial suppression of charm production. Thus we find that while the inclusion of mere multiple scattering can lead to increase in production of charm at intermediate p_T, the inclusion of gluon emission rapidly depletes the momenta of the partons. Please note that this significant energy loss is due to vacuum radiation matrix elements, since the PCM does not contain any medium-modified matrix elements. Please also note that the presence of hydrodynamic flow would significantly alter the shape of R_{AA} at low transverse momenta.

In Fig. 18, we show a comparison of the nuclear modification factor $R_{\rm AA}$ for central collisions at central rapidity. Interestingly, we find a significant suppression, even down to intermediate p_T, indicating that charm interactions in the early nonequilibrium phase of the reaction play a significant role. Clearly, the PCM calculation of $R_{\rm AA}$ suppression is less than observed in the data; i.e., it cannot account for the full suppression observed. Also, the radial flow bump at low p_T is missing in the PCM calculation. Yet our results indicate that a comprehensive calculation of heavy flavor energy loss would need to account for both the early time dynamics as described by the PCM as well as the later time dynamics as described by some form of hydrokinetic transport [20,22,26,35,69]. Please note that the experimental data are for 0–10% centrality while our calculations are for impact parameter equal to zero.

IV. SUMMARY

We have studied the production and scattering of heavy quarks in the parton cascade model and presented results for

production of charm quarks in pp and Au + Au collisions at $\sqrt{s_{NN}} = 200$ GeV. We have verified the PCM implementation by comparing an eikonal approximation implementation against an independent calculation using the formalism of minijets. The effect of charm-medium interactions is studied by successively opening up reaction channels, starting with only primary-primary collisions at first, then allowing for multiple scatterings, and finally switching on multiple scatterings along with parton splittings. Interestingly, while the last named calculations lead to a very large increase in multiple collisions, the charm production does not increase by the same factor, mainly due to their production threshold as the initial light partons lose energy while radiating gluons. The space-time distribution of the production vertices of charm quarks provide valuable insight into the production process. The transverse momentum spectrum obtained using the complete calculation is found to have a shape similar to the experimental results, confirming the importance of radiative energy loss suffered by heavy quarks at intermediate and large p_T. Results for different systems, energies, and centralities would provide very valuable confirmations of our procedure and findings. The considerable suppression of production of charm quarks having large transverse momenta due to the multiple collisions and radiations seen in the present work suggests that a significant contribution to jet quenching could also arise from the same mechanism. This is under investigation.

ACKNOWLEDGMENTS

D.K.S. gratefully acknowledges the support by the Department of Atomic Energy, India. This research was supported in part by the ExtreMe Matter Institute (EMMI) at the GSI Helmholtzzentrum für Schwerionenforschung, Darmstadt, Germany. We thankfully acknowledge the High Performance Computing Facility of Variable Energy Cyclotron Centre Kolkata for all the help during these calculations performed over several months. S.A.B. acknowledges support by US Department of Energy Grant No. DE-FG02-05ER41367.

[1] M. Gyulassy and L. McLerran, Nucl. Phys. A **750**, 30 (2005).
[2] B. Muller and J. L. Nagle, Annu. Rev. Nucl. Part. Sci. **56**, 93 (2006).
[3] B. Muller, J. Schukraft, and B. Wyslouch, Annu. Rev. Nucl. Part. Sci. **62**, 361 (2012).
[4] X.-N. Wang (ed.), *Quark-Gluon Plasma 5* (World Scientific, Singapore, 2016).
[5] P. F. Kolb and U. W. Heinz, arXiv:nucl-th/0305084.
[6] H. Song, S. A. Bass, U. Heinz, T. Hirano, and C. Shen, Phys. Rev. Lett. **106**, 192301 (2011).
[7] B. Alver *et al.* (PHOBOS Collaboration), Phys. Rev. Lett. **104**, 142301 (2010).
[8] B. Alver, B. B. Back, M. D. Baker, M. Ballintijn, D. S. Barton, R. R. Betts, R. Bindel, W. Busza, V. Chetluru, E. Garcia *et al.*, Phys. Rev. C **77**, 014906 (2008).
[9] B. Alver and G. Roland, Phys. Rev. C **81**, 054905 (2010); **82**, 039903(E) (2010).
[10] R. J. Fries, B. Muller, C. Nonaka, and S. A. Bass, Phys. Rev. Lett. **90**, 202303 (2003).
[11] V. Greco, C. M. Ko, and P. Levai, Phys. Rev. Lett. **90**, 202302 (2003).
[12] B. Svetitsky, Phys. Rev. D **37**, 2484 (1988).
[13] M. G. Mustafa, D. Pal, and D. K. Srivastava, Phys. Rev. C **57**, 889 (1998).
[14] M. G. Mustafa, D. Pal, D. K. Srivastava, and M. Thoma, Phys. Lett. B **428**, 234 (1998).
[15] M. Gyulassy, P. Levai, and I. Vitev, Phys. Rev. Lett. **85**, 5535 (2000).
[16] M. Djordjevic and M. Gyulassy, Nucl. Phys. A **733**, 265 (2004).
[17] G. D. Moore and D. Teaney, Phys. Rev. C **71**, 064904 (2005).
[18] S. Peigne and A. Peshier, Phys. Rev. D **77**, 114017 (2008).
[19] S. K. Das, J.-E. Alam, and P. Mohanty, Phys. Rev. C **82**, 014908 (2010).
[20] P. B. Gossiaux, J. Aichelin, T. Gousset, and V. Guiho, J. Phys. G **37**, 094019 (2010).
[21] R. Abir, U. Jamil, M. G. Mustafa, and D. K. Srivastava, Phys. Lett. B **715**, 183 (2012).
[22] S. K. Das, F. Scardina, S. Plumari, and V. Greco, Phys. Lett. B **747**, 260 (2015).
[23] M. Younus and D. K. Srivastava, J. Phys. G **37**, 115006 (2010).
[24] S. Cao, G.-Y. Qin, and S. A. Bass, Phys. Rev. C **88**, 044907 (2013).
[25] H. van Hees, M. Mannarelli, V. Greco, and R. Rapp, Phys. Rev. Lett. **100**, 192301 (2008).
[26] R. Rapp and H. van Hees, Heavy quarks in the quark-gluon plasma, in *Quark-Gluon Plasma 4*, edited by R. C. Hwa and X.-N. Wang (World Scientific, Singapore, 2010), pp. 111–206.
[27] A. Andronic, F. Arleo, R. Arnaldi, A. Beraudo, E. Bruna, D. Caffarri, Z. Conesa del Valle, J. G. Contreras, T. Dahms, A. Daines *et al.*, Eur. Phys. J. C **76**, 107 (2016).
[28] G. Xie (STAR Collaboration), Nucl. Phys. A **956**, 473 (2016).
[29] W. Cassing, E. L. Bratkovskaya, and A. Sibirtsev, Nucl. Phys. A **691**, 753 (2001).
[30] E. L. Bratkovskaya, W. Cassing, and H. Stocker, Phys. Rev. C **67**, 054905 (2003).
[31] E. L. Bratkovskaya, W. Cassing, H. Stocker, and N. Xu, Phys. Rev. C **71**, 044901 (2005).
[32] O. Linnyk, E. L. Bratkovskaya, and W. Cassing, Nucl. Phys. A **807**, 79 (2008).
[33] O. Linnyk, E. L. Bratkovskaya, and W. Cassing, Int. J. Mod. Phys. E **17**, 1367 (2008).
[34] T. Song, H. Berrehrah, D. Cabrera, J. M. Torres-Rincon, L. Tolos, W. Cassing, and E. Bratkovskaya, Phys. Rev. C **92**, 014910 (2015).
[35] T. Song, H. Berrehrah, D. Cabrera, W. Cassing, and E. Bratkovskaya, Phys. Rev. C **93**, 034906 (2016).
[36] P. Levai, B. Muller, and X.-N. Wang, Phys. Rev. C **51**, 3326 (1995).
[37] Z.-W. Lin and M. Gyulassy, Phys. Rev. C **51**, 2177 (1995); **52**, 440 (1995).
[38] M. L. Mangano, P. Nason, and G. Ridolfi, Nucl. Phys. B **373**, 295 (1992).
[39] S. Frixione, M. L. Mangano, P. Nason, and G. Ridolfi, Adv. Ser. Dir. High Energy Phys. **15**, 609 (1998).

[40] M. Younus, U. Jamil, and D. K. Srivastava, J. Phys. **39**, 025001 (2012).
[41] M. He, R. J. Fries, and R. Rapp, Phys. Rev. C **86**, 014903 (2012).
[42] P. B. Gossiaux *et al.*, arXiv:1102.1114.
[43] J. Uphoff, O. Fochler, Z. Xu, and C. Greiner, Phys. Lett. B **717**, 430 (2012).
[44] F. Scardina, S. K. Das, S. Plumari, D. Perricone, and V. Greco, J. Phys. Conf. Ser. **535**, 012019 (2014).
[45] J. Uphoff, O. Fochler, Z. Xu, and C. Greiner, J. Phys. G **42**, 115106 (2015).
[46] K. Geiger and B. Muller, Nucl. Phys. B **369**, 600 (1992).
[47] K. Geiger, Phys. Rev. D **46**, 4965 (1992).
[48] K. Geiger, Phys. Rev. D **46**, 4986 (1992).
[49] K. Geiger, Phys. Rev. D **48**, 4129 (1993).
[50] K. Geiger and J. I. Kapusta, Phys. Rev. D **47**, 4905 (1993).
[51] K. Geiger, Phys. Rep. **258**, 237 (1995).
[52] S. A. Bass, B. Muller, and D. K. Srivastava, Phys. Lett. B **551**, 277 (2003).
[53] M. Younus, C. E. Coleman-Smith, S. A. Bass, and D. K. Srivastava, Phys. Rev. C **91**, 024912 (2015).
[54] Z. Xu and C. Greiner, Phys. Rev. C **71**, 064901 (2005).
[55] S. Cao and S. A. Bass, Phys. Rev. C **84**, 064902 (2011).
[56] B. Combridge, Nucl. Phys. B **151**, 429 (1979).
[57] J. C. Collins, D. E. Soper, and G. F. Sterman, Nucl. Phys. B **263**, 37 (1986).
[58] Z. B. Kang, F. Ringer, and I. Vitev, J. High Energy Phys. 03 (2017) 146.
[59] T. Sjostrand, Phys. Lett. B **157**, 321 (1985).
[60] G. Altarelli and G. Parisi, Nucl. Phys. B **126**, 298 (1977).
[61] E. Eichten, I. Hinchliffe, K. D. Lane, and C. Quigg, Rev. Mod. Phys. **56**, 579 (1984); **58**, 1065 (1986).
[62] M. Glück, E. Reya, and A. Vogt, Z. Phys. C **67**, 433 (1995).
[63] Z. Ye (STAR Collaboration), Nucl. Phys. A **932**, 45 (2014).
[64] L. Adamczyk *et al.* (STAR Collaboration), Phys. Rev. Lett. **113**, 142301 (2014).
[65] G. Xie (STAR Collaboration), Nucl. and Part. Phys. Proc. **289–290**, 209 (2017).
[66] R. Vogt, B. V. Jacak, P. L. McGaughey, and P. V. Ruuskanen, Phys. Rev. D **49**, 3345 (1994).
[67] S. J. Brodsky, P. Hoyer, A. H. Mueller, and W.-K. Tang, Nucl. Phys. B **369**, 519 (1992).
[68] C. Peterson, D. Schlatter, I. Schmitt, and P. M. Zerwas, Phys. Rev. D **27**, 105 (1983).
[69] S. Cao, Y. Huang, G.-Y. Qin, and S. A. Bass, J. Phys. G **42**, 125104 (2015).